Mass and heat transfer modeling of bio-substrates during packaging

Maria Valeria De Bonis, Maria Cefola, Bernardo Pace & Gianpaolo Ruocco

Heat and Mass Transfer
Wärme- und Stoffübertragung

ISSN 0947-7411
Volume 49
Number 6

Heat Mass Transfer (2013) 49:799-808
DOI 10.1007/s00231-013-1122-2

Springer

Heat Mass Transfer (2013) 49:799–808
DOI 10.1007/s00231-013-1122-2

ORIGINAL

Mass and heat transfer modeling of bio-substrates during packaging

Maria Valeria De Bonis · Maria Cefola · Bernardo Pace · Gianpaolo Ruocco

Received: 12 July 2012 / Accepted: 13 February 2013 / Published online: 2 March 2013

Abstract Perishable bio-substrate behavior can be modeled during packaged storage. Local mass and heattransfer have been coupled to respiration rate and microbial growth. Validating measurements have also been performed, and a multi-objective optimization was employed to tune the model. The model is able to simulate gas composition history and local bacteria spoilage in storage modes commonly adopted by the food industry, depending on product features and temperature. Exploitation of this mathematical tool would allow for informed technical and management decisions.

List of symbols

a	Ambient domain
A	Surface (m^2)
A_1	Pre-exponential term (1/s)
A_2	Exponential factor (m^3/mol)
c	Concentration (mol/m^3 or %)
c_p	Specific heat (J/kgK)
D	Mass diffusivity (m^2/s)
f	Packaging film
h	Head space domain
J	Flow of gas (mol/m^2s)
k	Thermal conductivity (W/mK)
K	Kinetics coefficient (1/s)
n	Normal versor
MS	Mesophilic bacteria
p	Packaging tray, process
PS	Psychrophilic bacteria
s	Substrate domain
t	Time (s)
T	Temperature (K)
u	CFU (Log CFU/g)
V	Volume (m^3)

Greek

α	Empirical constant
ρ	Density (kg/m^3)

Subscripts

a	Ambient
f	Packaging film
h	Head space
i	Initial, reference
MS	Mesophilic bacteria
p	Packaging tray, process
PS	Psychrophilic bacteria
r	Respiration
s	Substrate

M. V. De Bonis · G. Ruocco
CFDINNOVA/BI CUBE, Centro Direzionale Franco/Area C, 85100 Potenza, Italy

M. V. De Bonis · G. Ruocco (✉)
Scuola d'Ingegneria, Università degli Studi della Basilicata, Campus Macchia Romana, 85100 Potenza, Italy
e-mail: gianpaolo.ruocco@unibas.it
URL: www.CFDINNOVA.com

M. Cefola · B. Pace
Institute of Sciences of Food Production, National Research Council (CNR), Via G. Amendola 122/O, 70126 Bari, Italy

1 Introduction

The food engineering has been gaining increasing recognition due to its contribution to innovative products and their manufacturing processes. To this end, mass, heat and momentum transfers can be usefully studied and speculated. The discipline shows its complexity as all transport

phenomena can be intertwined and non-linearly interdependent [4].

In the food engineering framework, packaging is essential to ensure main features in perishable substrate (such as safety and quality in foods), protecting from contamination and spoilage, and also easing transportation and storage. Commonly, with the Modified Atmosphere Packaging (MAP) the gas composition in the space around the substrate (head space) is modified from normal air in order to prolong the duration and maintain original features. MAP slows down the natural deterioration of the substrate when respiration is present, but other metabolic or supplementary degrading factors should be taken into account.

As recently summarized by Zhuang [20], MAP may be achieved either actively or passively (aMAP or pMAP), depending on the allowed gas before package sealing, which in the former case is renewed and controlled by an attached system. In both modes, the head space composition modifies during storage as a consequence of the substrate's respiration and/or the metabolism of associated microorganisms, and the inherent permeation of gases through the packaging material. At the end, the substrate duration will depend on the equilibrium between the inherent metabolism and the package permeation rates for O_2 and CO_2 [8, 10].

As MAP undergoes commonplace adoption and rapid development and exploitation in the food industry, research on identifying optimal MAP conditions (including packaging types and sizes, selective permeability films, and storage conditions) may rely on advanced predicting technologies, that may prove as an economic method to evaluate MAP performance and substrate duration. To this end, the importance of an analytical approach based on the heat and mass transfer equations has been recently proposed by Piringer [14] and Zhang et al. [19]. Generally, a multidimensional computational framework may offer many benefits when simulating a complex geometry/multiphysics configuration, specially when interdependencies among the governing variables occur.

In simulating the evolution of bio-substrates in packaging, multidimensional diffusive modeling by partial differential equations (PDEs) has been rarely employed. Lammertyn et al. [11] and Opara and Zou [12] used PDEs but their works did not deal with MAPs. Some preliminary results with PDEs were reported by De Bonis and Ruocco [4]. In the present work, the complete modeling approach is presented with reference to the evolution of the head space composition for a selected model food (peeled ellipsoid cactus pears), including the effect of respiration and additional metabolic mechanisms. The model choice is justified by flesh homogeneity and structure uniformity. The minimal processing (peeling) increases the fruits' degradative process.

Different storage temperatures and gas compositions have been tried and validated successfully, for the first time, by comparing with the associated experiments, to yield for a model which is generally applicable to any general packaging configuration and condition. No empirical assumptions were adopted, whereas chemical and biological constants were derived by a special optimization procedure, based on comparison with the corresponding experimental results.

2 Model formulation

Fruit evolution in MAP relies on the mass transfer mechanisms depicted in Fig. 1. The mechanisms are arranged on a series mode. So let us start from the rightmost domain, the subject substrate, *s*.

Due to respiration, a flux of O_2 is absorbed through a first domain interface (substrate's external surface, represented by the thick vertical line at right), and converted into CO_2 (these two fluxes are represented in Fig. 1 by horizontal arrows through the external surface). Moreover, in domain *s* the gas species are internally diffused due to mass transfer (represented by vertical arrows).

Then let us consider the leftmost domain, the surrounding ambient, *a*. Due to diffusion through a second interface (the packaging film, represented by the thick vertical line at left) a gas mixture exchange also occur with the ambient domain, *a* (these two fluxes are represented in Fig. 1 by horizontal arrows through the packaging film).

The composition of the head space domain, *h*, is then determined by the make-up of the resulting mass transfer through the interfaces, as mentioned above. Moreover, in this domain the gas species are also internally diffused due to mass transfer (represented by vertical arrows).

The present paper addresses the modeling and validation of the *h*/*s* ensemble domain, based on said interrelated mechanisms. Furthermore, the *s* domain is also subject to microbial growth, which depends on the inherent temperature regime, affecting in turn the depletion of oxygen in the ensemble. The biochemical evolution is simulated for a number of aMAP and pMAP cases, at constant temperature, as consistent with the related food industry procedures. A 3D rendering of the package, containing 3 fruits, and a transversal section of the package and fruit ensemble is shown in Fig. 2.

2.1 Assumptions

According to the above description of the various mechanisms, a number of assumptions are considered, referring to the *a*, *h* and *s* domains (Fig. 1):

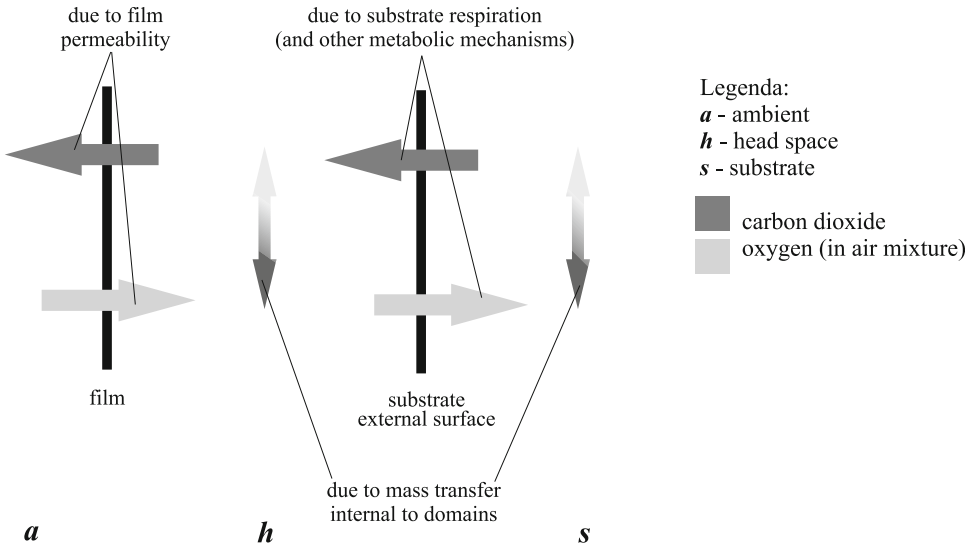

Fig. 1 Schematic of the subject *a*, *h* and *s* domains, and the inherent diffusive transfers

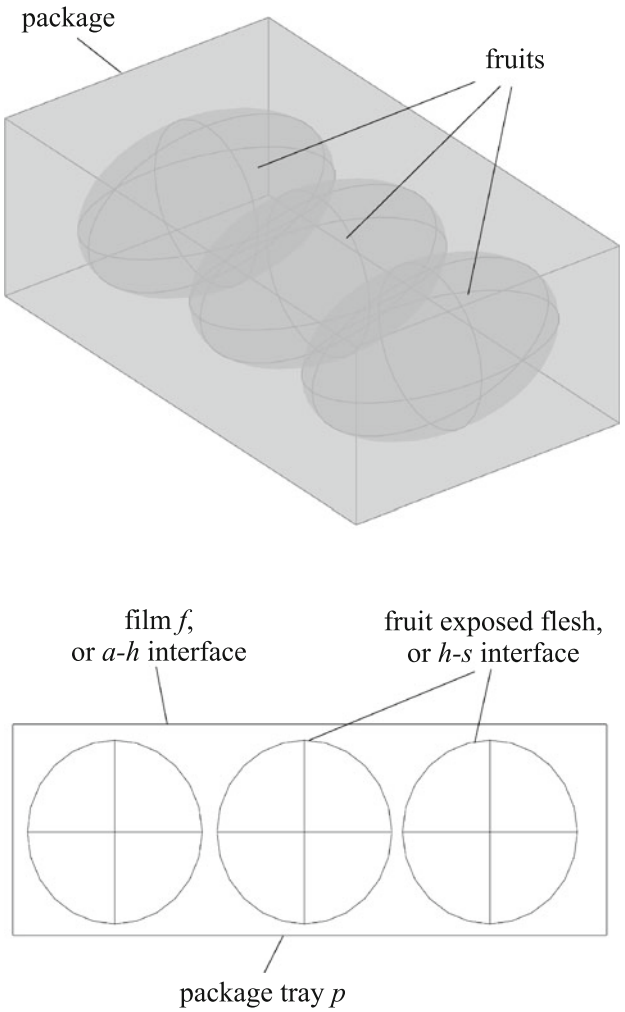

Fig. 2 *Top* The package and fruit ensemble. *Bottom* A central/transversal section of the package

- No modification in the fruits flesh is accounted for, due to peeling
- Two bacteria populations (mesophilic, *MS*, and psychrophilic, *PS*, as suggested by Cefola et al. [2]) are accounted for in *s*, based on their specific metabolism
- Initially, the gas is distributed uniformly in both *h* and *s*
- Gas continuity is allowed for through the food external surface ($h-s$ interface)
- The fruits are placed in the package at their initial temperature, then are cooled down to a given storage condition
- The inherent thermal fluxes and head space height are considered to be small enough to ensure that no thermal gradients are formed in *h*, then no buoyancy (natural convection) is considered
- The presence of moisture is neglected in *h*, and no heat source or sink is accounted for, due to substrate respiration or moisture condensation
- No heat generation is considered in the fruits, due to the adopted temperature regime
- All thermophysical properties are taken as constant or piecewise constant, as required
- Modeling is not carried out in *a*, and no thermal transfer at the $a-h$ interface is accounted for

2.2 Governing equations

With reference to the previous statements, the governing equations for the diffusion of the gas species and heat conduction in vector form, as modified from [1], are applied to each domain to yield for the distributions of the gas molar concentration, *c*, and temperature, *T*. Similarly,

the evolution of the microbial species is applied to the s domain, to yield for the distributions of their colony forming units (CFU), u.

– In the head space: *Continuity*, O_2:

$$\frac{\partial c_{O_2}}{\partial t} + \nabla \cdot \left(-D_{O_2,h} \nabla c_{O_2}\right) = 0 \quad (1)$$

Continuity, CO_2:

$$\frac{\partial c_{CO_2}}{\partial t} + \nabla \cdot \left(-D_{CO_2,h} \nabla c_{CO_2}\right) = 0 \quad (2)$$

Energy:

$$\rho_h c_{ph} \frac{\partial T}{\partial t} + \nabla \cdot (-k_h \nabla T) = 0 \quad (3)$$

– In the substrate: *Continuity*, O_2:

$$\frac{\partial c_{O_2}}{\partial t} + \nabla \cdot \left(-D_{O_2,s} \nabla c_{O_2}\right) = -\alpha_{O_2} K_r c_{O_2} \quad (4)$$

Continuity, CO_2:

$$\frac{\partial c_{CO_2}}{\partial t} + \nabla \cdot \left(-D_{CO_2,s} \nabla c_{CO_2}\right) = \alpha_{CO_2} K_r c_{O_2} \quad (5)$$

Energy:

$$\rho_s c_{ps} \frac{\partial T}{\partial t} + \nabla \cdot (-k_s \nabla T) = 0 \quad (6)$$

Continuity, MS:

$$\frac{\partial u_{MS}}{\partial t} + \nabla \cdot (-D_{MS} \nabla u_{MS}) = K_{MS} u_{MS} \quad (7)$$

Continuity, PS:

$$\frac{\partial u_{PS}}{\partial t} + \nabla \cdot (-D_{PS} \nabla u_{PS}) = K_{PS} u_{PS} \quad (8)$$

All thermophysical properties, as suggested by the available literature, are constant with temperature and are reported in Table 1, with the composition of the selected substrate taken from [15]. The source terms at the right hand sides of Eqs. (4, 5, 7, 8), related to the creation or destruction of the chemical species or microorganisms, are inferred upon next.

2.3 Respiration and metabolism rates in the source terms

In this work, a kinetics-based approach is employed to come up with the source terms in Eqs. (4, 5, 7, 8), depending on the adopted packaging configuration. All constants have been determined based on a special optimization procedure, as described later in Sect. 3.2

A large deal of work can be found on discrete MAP modeling, as reviewed by Fonseca et al. [7]. To deal with kinetics of various kind, a simplified Michaelis–Menten relationship (depending on the local c_{CO2}) is adopted, as in [5]:

$$K_r = A_1 \exp(-A_2 c_{CO_2}) \quad (9)$$

whose optimized constants A_1 and A_2, reported in Table 2, account for the CO_2-induced respiration inhibition. In order to include the residual metabolism or additional deteriorative reactions promoted by the oxygen (such as pigment oxidation, senescence, enzymatic reactions and so on [16]), an empirical optimized constant α dependent on the gas species has been included at the right hand sides of Eqs. (4, 5). The adopted values of constants α are reported in Table 2.

Furthermore, for the first time, a microorganism kinetics in a MAP modeling framework is included in this paper. The importance of the microbiological and biochemical stability of fresh-cut fruit is assessed by many sources, including Soliva-Fortuny et al. [18]. Moreover, most of the common spoilage bacteria and fungi require oxygen for

Table 1 Values of thermophysical properties and diffusion coefficients for the considered model food

Parameter	Value	References
$D_{O_2,f}$ (m^2/s)	1.29×10^{-16}	Piergiovanni and Limbo [13]
$D_{CO_2,f}$ (m^2/s)	7.16×10^{-17}	Piergiovanni and Limbo [13]
$D_{O_2,h}$ (m^2/s)	1.78×10^{-5}	Singh and Heldman [17]
$D_{CO_2,h}$ (m^2/s)	1.38×10^{-5}	Singh and Heldman [17]
$D_{O_2,s}$ (m^2/s)	1.00×10^{-8}	Lammertyn et al. [11]
$D_{CO_2,s}$ (m^2/s)	1.00×10^{-8}	Lammertyn et al. [11]
D_{MS} (m^2/s)	1.4×10^{-12}	Dense and Van Impe [6]
D_{PS} (m^2/s)	1.4×10^{-12}	Dense and Van Impe [6]
c_{ph} (J/kgK)	1,100	Singh and Heldman [17]
k_h (W/mK)	0.024	Singh and Heldman [17]
ρ_h (kg/m^3)	1.206	Singh and Heldman [17]
c_{ps} (J/kgK)	3,793	Singh and Heldman [17]
k_s (W/mK)	0.40	Singh and Heldman [17]
ρ_s (kg/m^3)	920	Singh and Heldman [17]

Table 2 Values of model constants for respiration and microbial kinetics, depending on the MAP mode and for two different temperatures

Parameter	aMAP at $T_p = 4$ °C	aMAP at $T_p = 8$ °C	pMAP at $T_p = 8$ °C
A_1	1.00×10^{-6}	1.00×10^{-6}	1.00×10^{-6}
A_2	2.84×10^{-3}	2.84×10^{-3}	2.84×10^{-3}
α_{O2}	5.0	9.5	8.5
α_{CO2}	2.9	8.5	7.5
A_{MS}	5.61×10^{31}	2.60×10^{32}	2.90×10^{32}
A_{PS}	6.33×10^{31}	2.80×10^{32}	3.50×10^{32}
$E_{a,MS}$	2.029×10^5	2.029×10^5	2.029×10^5
$E_{a,PS}$	2.029×10^5	2.012×10^5	2.012×10^5

growth [11, 16], therefore affecting the evolution of the gas composition in the head space. Then, K_{MS} and K_{PS} in Eqs. (7, 8) were found to account for the dependence of the temperature and oxygen bio-availability, by means of another modified Arrhenius kinetics:

$$K_{MS} = A_{MS} \exp\left(\frac{-E_{a,MS}}{RT}\right)\left(\frac{c_{O_2}}{c_{O_2,i}}\right) \quad (10)$$

$$K_{PS} = A_{PS} \exp\left(\frac{-E_{a,PS}}{RT}\right)\left(\frac{c_{O_2}}{c_{O_2,i}}\right) \quad (11)$$

whose optimized constants are also reported in Table 2. All optimized parameters are constant with temperature within each aMAP and pMAP run, as needed.

2.4 Initial and boundary conditions

Initial conditions:

- in s the gas concentrations are initially set at their atmospheric values, while in h they are set at given c_{O2},i and c_{CO2},i values
- the temperature is set at a given T_i value in both h and s
- the bacteria counts are initially set at their experimental values ($u_{MS} = 0.71$CFU, $u_{PS} = 0.029$ CFU)

Boundary conditions (Fig. 2):

- at the film boundary (the $a-h$ interface or f boundary), two different gas fluxes are applied depending on their respective atmospheric values and the specific diffusion coefficient in the film matrix, which commonly happens to be selective with respect to the given species (as will be referred upon later):

$$\mathbf{J}_{O_2} = \mathbf{n} \cdot \left(D_{O_2,f} \nabla c_{O_2}\right) \quad (12)$$

$$\mathbf{J}_{CO_2} = \mathbf{n} \cdot \left(-D_{CO_2,f} \nabla c_{CO_2}\right) \quad (13)$$

- at the package tray (the p boundary), an impermeability condition is applied for each gas species:

$$\mathbf{n} \cdot \left(D_p \nabla c_{O_2}\right) = 0, \qquad \mathbf{n} \cdot \left(D_p \nabla c_{CO_2}\right) = 0 \quad (14)$$

- all around the package (along the f and p boundaries) a given temperature condition is applied:

$$T = T_p \quad (15)$$

- at the $h-s$ interface, the gas flux continuity and energy conservation are imposed, while an insulation condition is applied for each microbial species:

$$\mathbf{n} \cdot (D_{MS} \nabla u_{MS}) = 0, \qquad \mathbf{n} \cdot (D_{PS} \nabla u_{PS}) = 0 \quad (16)$$

The ideal gas law was used for the conversion of the units from gas molar concentrations to gas partial pressures and percentages, as proposed also by Lammertyn et al. [11].

3 Materials and methods

3.1 Validation experiments

Fruits were washed in tap water, sanitized by immersion in 200 mg/kg of NaClO for 5 min, and left to dry at room temperature. Then three peeled fruits (about 300 g) for each replication were set in PET 14 × 9 × 5 cm^3 trays (model C250/50 Carton Pack, Rutigliano, Italy) and sealed (Boxer 50, Lavezzini Vacuum Packaging System, Fiorenzuola d'Arda, Italy) in polyamide/polyethylene (PA/PE) plastic bags (O_2 permeability 40 cm^3 m^2 day^{-1} bar^{-1}, thickness 140 μm, Orved, Musile di Piave, Italy).

In this work, either aMAP (10 % for both O_2 and CO_2) or pMAP (sealed in ambient air, 20 % for O_2 and 0.003 % for CO_2) trials were performed, the former at both 4 and 8 °C, the later at 8 °C only. Unpackaged triplicate samples (i.e. trays in unsealed plastic bags) were used as control. Samples were stored for different durations: 3, 6, 9 or 13 storage days. Then a total of 12 packages (3 replications for 4 durations) for each treatment (MAP modes, control, and temperature) were prepared.

The composition of gas mixture in h was sampled at the initial time and after 9 h and 1, 2, 3, 6, 7, 10 and 13 days (or 24, 48, 72, 144, 168, 240 and 312 h), by using an infrared (CO_2) and paramagnetic (O_2) gas analyzer (CheckPoint, PBI-Dansensor, Rønnedevej, Denmark). A needle was inserted into the package through a rubber seal placed onto the film to sip out 1 mL of gas sample each time. At each considered sampling time, standard deviations of gas concentrations were also calculated.

For each replication 30 g of fruit (averaging between surface and core flesh) was then transferred aseptically into a Stomacher bag containing 90 mL of sterile saline solution (9 mg/kg NaCl), homogenized for 1 min using a Stomacher machine (BagMixer, Interscience, St. Nom, France), and plated on Plate Count Agar (Oxoid, Milan, Italy) for total bacteria counts. The appropriate dilutions of homogenized samples were plated in triplicate. *MS* and *PS* bacteria were counted at the initial time and after 24 h and 7 days of growth at 30 and 7 °C, respectively.

3.2 Computations

The governing equation set, with associated initial and boundary conditions, was integrated by means of a computational fluid dynamics (CFD) commercial code [3]. A regular computational grid was adopted. The domains were discretized by Lagrange-quadratic elements. Several grids were tried, from about 1,000 tetrahedral elements up to more than 5,800. The final grid, yielding for grid-independency results, had some 2,000 elements. Each run was executed for a total elapsed period of about 13 days, taking

less than 3 min on a Supermicro PC carrying a Xeon (3 GHz) CPU, under Windows XP.

All source terms included in Eqs. (4, 5, 7, 8) play an important role, holding the non-linear and inter-dependence nature of the governing equations. Instead of using empirical values, as implied earlier, the model constants whose values are reported in Table 2 were subject to optimization by fitting the average computed values to the experimental data, with the same procedure proposed by De Bonis and Ruocco [4]. This was specially important for the α constants which account for the inherent asymmetry between gas fluxes, due to the fact that O_2 is subject to an additional sink, as mentioned above.

4 Results and discussion

4.1 Model validation: head space composition progress

The average computed values of c_{O2} and c_{CO2} in the head space have been preliminary compared with the associated experiments, for both pMAP and aMAP. In Fig. 3a the validation for pMAP at $T_p = 8$ °C with $T_i = 20$ °C is first presented. After 72 h (or 3 days), the O_2 level decreases down to about 3 %, with the CO_2 level increasing up to almost 14 % at a similar rate. Later on, the gas levels smooth down to their final values of 0.5 and 19 % for oxygen and carbon dioxide, respectively. The model performs nicely specially in the last part of the storage duration, with a maximum discrepancy of about 50 % with respect to the average experimental data, for carbon dioxide after about 24 h. It should be soon noted that the departure from classical exponential progress that the computations exhibit is given by the non-linear nature of the model and the optimization procedure explained earlier.

The model performs even better for the aMAP at the same T_p (Fig. 3b), where faster gas responses are detected after 48 h (reduction of oxygen and increment of carbon dioxide), attaining their final value of 0.2 and 20 % for oxygen and carbon dioxide, respectively.

The model shows its validity also in the last explored case, aMAP at $T_p = 4$ °C (Fig. 3c). In this case, the gas evolution in the head space is slower, with the oxygen level becoming constant after 7 days, and the carbon dioxide increasing only marginally.

4.2 Effect of MAP mode and process temperature on head space composition and sample progress

The results presented so far allow one to speculate on the oxygen/carbon dioxide asymmetrical makeup, which is one of the parameters at stake in MAP configurations. This can

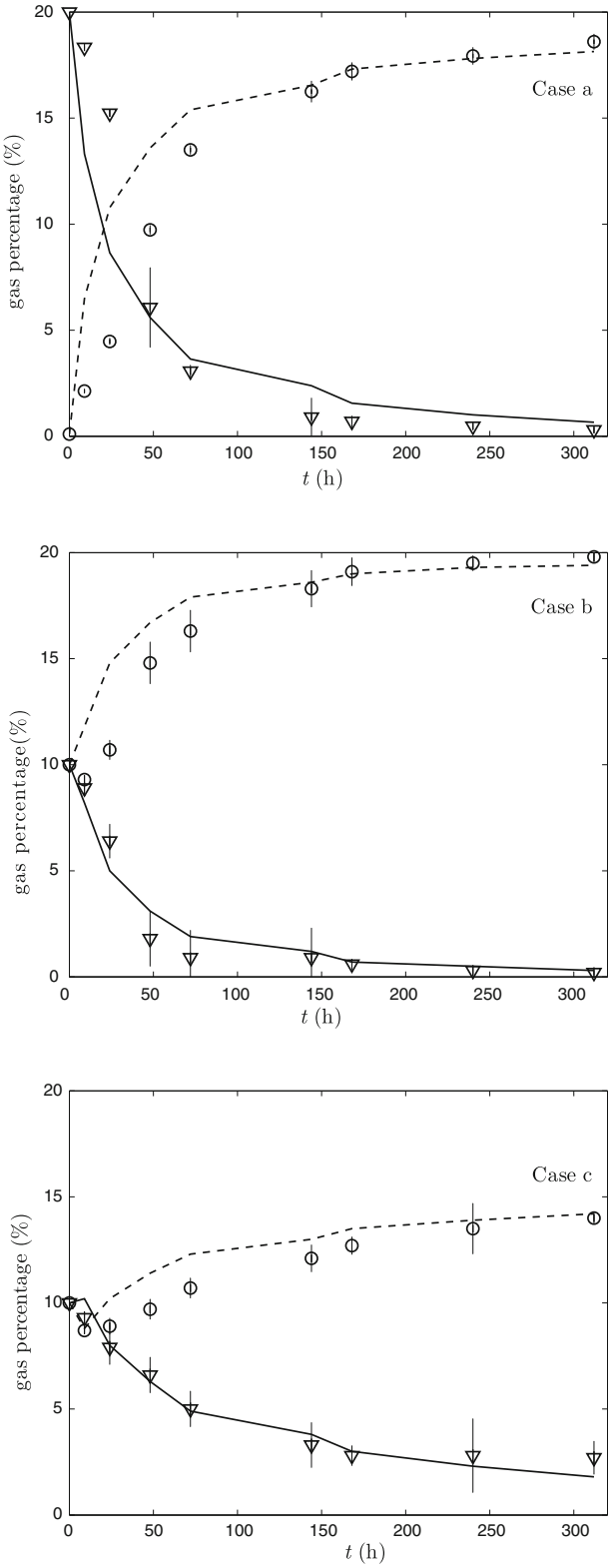

Fig. 3 Comparison between experimental (*inverted triangle*, with associated standard deviations) and numerical averaged (—) values of c_{O2} in *h*, and experimental (*circle*, with associated standard deviations) and numerical averaged (- -) values of c_{CO2} in *h*. Case **a**: pMAP at $T_p = 8$ °C; Case **b**: aMAP at $T_p = 8$ °C; Case **c**: aMAP at $T_p = 4$ °C. The optimized model describes correctly the progress of gas composition in a package, in presence of substrates with residual metabolism

be done by inferring upon the effect of the MAP mode and storage temperature.

Figure 3a, b can be scrutinized again in order to compare the MAP modes. In pMAP (Fig. 3a), gas species in the h and s domains enjoy an initial equilibrium, that favors a smoother evolution than with an aMAP (Fig. 3b), where the concentration gradient in the packaging ensemble is higher instead. The present multidimensional model can indeed easily allows for computations of quantities such as the gas fluxes across a given surface. As an example, it is calculated that the O_2 flux across the $h-s$ interface is, at any given time, 5 orders of magnitude greater with aMAP than with pMAP. As a consequence it can be seen that, specially in the first storage hour, the mass transfer in aMAP is driven by species diffusion due to the higher concentration gradient, while in pMAP the respiration takes over determining the h composition.

It is also observed that the oxygen depletion is greater (about 12 %) than the associated carbon dioxide production, which is in agreement with the above speculation, and reflected in the α coefficients (Table 2) in right hand sides of Eqs. (4, 5). A much larger shift is detected in Fig. 3c, where O_2 depletion is larger than 70 % with respect to CO_2 production. This is apparently in contrast with the fact that the storage is cooler in this case, which should have limited the deteriorative effects that promote O_2 consumption.

Then, the CFD analysis can be exercised to inspect the gas concentration in the samples, which is indicative of the residual metabolism within the fruits and hence of product commercial life. In Fig. 4 the O_2 concentration distribution in pMAP after 13 days at $T_p = 8$ °C with $T_i = 20$ °C, is presented: c_{O2} is rather uniform, nevertheless a concentration minimum is somewhat still detected in the core of the fruits, due to the higher residual respiration and deteriorative reactions.

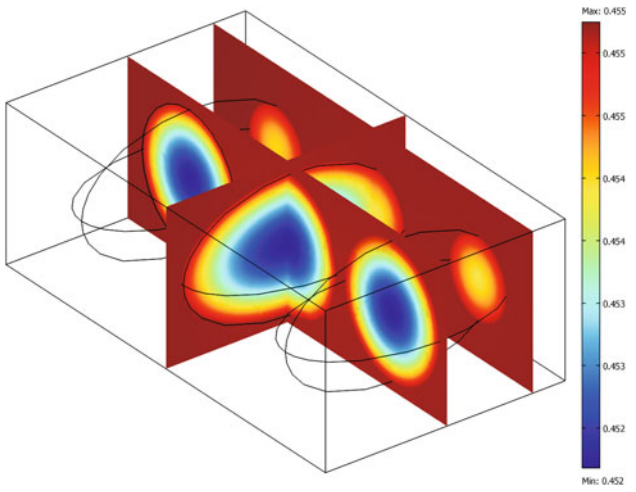

Fig. 4 The O_2 concentration distribution in pMAP after 13 days at $T_p = 8$ °C. The model allows to inspect the internal behavior of perishable substrates

4.3 Model validation: microbial proliferation progress

The model has also been validated by comparing its average computed values of microbial concentration (u_{MS} and u_{PS}) with the associated experiments, for both aMAP and pMAP modes, at $T_p = 8$ °C, still with $T_i = 20$ °C. In Fig. 5 (top) the validation for the aMAP is first presented. The predictive performance of microbial growth (averaged across the fruit volume) is always very good for *PS* (at right), while a consistent difference (about 50 %) is found at 150 h for *MS* (at left). It is evident that the aMAP fails to inhibit the *MS* growth, as the count exceeds 9 CFU at the final storage time. The adopted $T_p = 8$ °C is sufficient to limit the growth of *PS* instead, to a final value of about 6 CFU.

In Fig. 5 (bottom) the validation for the pMAP is then presented. Predictions are very good for both microbial species. In this case the combined microbial stability is improved, with a final value exceeding 7 CFU for both microbial species.

A possible exploitation of the presented comprehensive model is finally shown in Figs. 6 and 7: it is seen that MAPs can be effectively employed to inhibit microbial proliferation and extend food commercial life, and that a comprehensive transfer phenomena model such as the present one may represent a valid tool for the related industry. The CFD indeed allows one to inspect various scenarios unavailable otherwise.

3D microbial maps (u_{MS}) are first reported in Fig. 6, at final storage time for pMAP, for three wholesome samples (top), and when one of the fruits is superficially damaged and infected (bottom). At the damage site, a 4-fold bacterial contamination has been assumed, with respect to the original case. It is first seen that u_{MS} distribution depends on process cooling, from $T_i = 20$ °C to $T_p = 8$ °C: in the area where the fruits are closer (and thermal inertia greater) i.e. between left and central fruits, the temperature decreases less rapidly so that MS proliferation is greater (up to 6.9 CFU). Figure 6, bottom shows the distribution of u_{MS} with a damaged central fruit. It is clear in this case that the MAP inhibits the contamination: as O_2 level (shown earlier in Figs. 3 and 4) after 13 days is very low, bacterial growth and diffusion is inhibited. Therefore the contamination is limited to the wound area, and the microbial concentration elsewhere is unaffected.

A situation in which the ensemble with the infected sample is stored in atmospheric air instead (i.e. in an open box) is shown in Fig. 7. In this case, the value of maximum MS contamination reached 5.1 CFU after just 3 days of storage (top). After 4 days the entire package is strongly contaminated (bottom), with a maximum value of 16 CFU

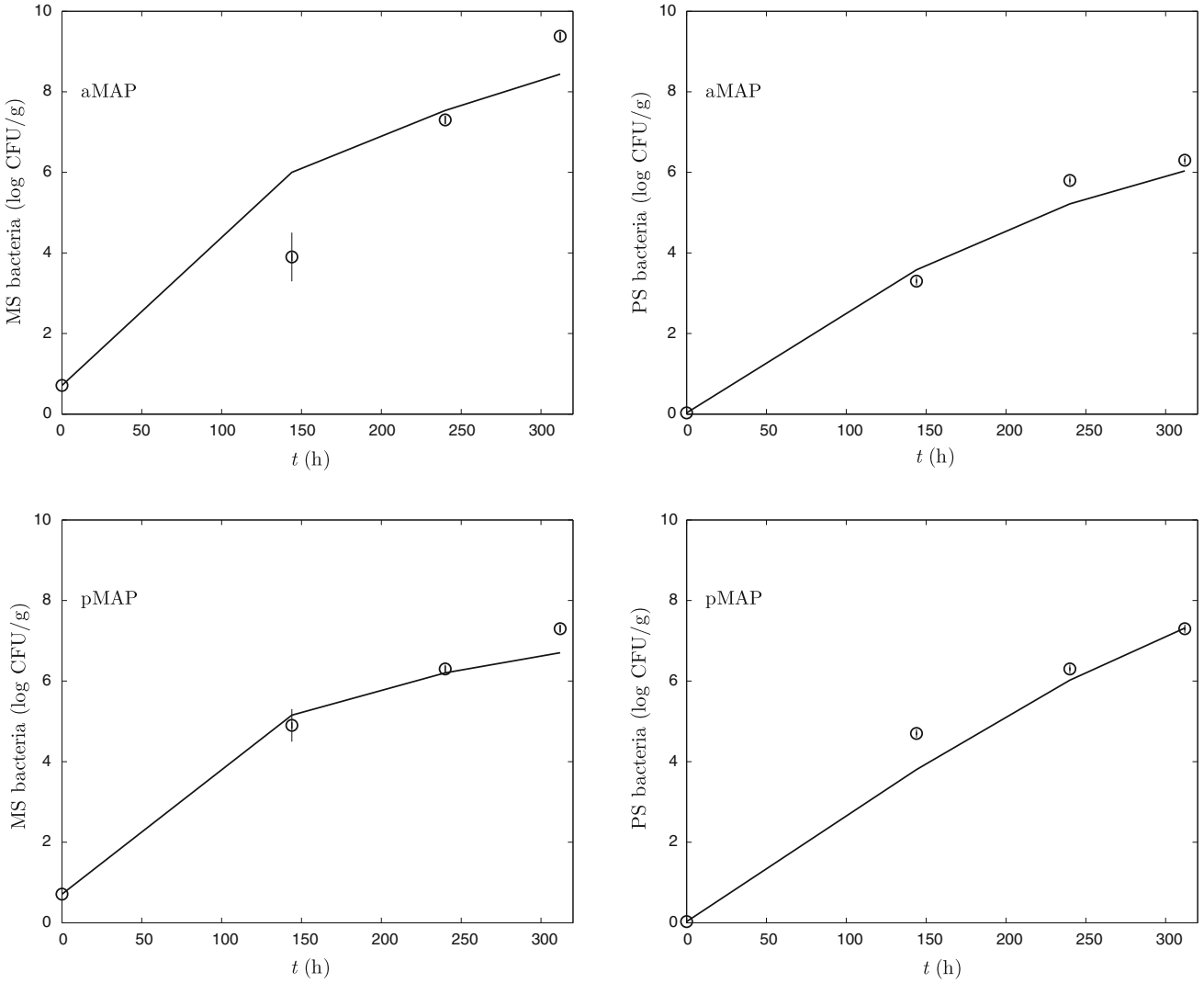

Fig. 5 Comparison between experimental (◯, with associated standard deviations) and computed (—) values of *MS* (*left*) and *PS* (*right*) CFU at $T_p = 8$ °C. *Top* aMAP; *bottom* pMAP. The model performs well in most cases, and is able to describe the microbial growth

with exceeds the safety limit (commonly assumed equal to 7 CFU).

5 Conclusions

In this work a multidimensional, transient model has been proposed by combining generalized mass and heat transfer notations, with respiration and microbial growth kinetics. The adoption of a predictive and comprehensive mathematical model is an economic method to evaluate packaging performance, compared to more expensive experimental methods.

The model has been applied to modified active and passive storage atmospheres of fresh produce packaging, and local concentrations of gas and microbial species, as well as local temperature, have been computed. A certain non-uniformity of microbial growth, due to the inherent temperature distribution, and a discordance of depleted oxygen with respect to the carbon dioxide, have been confirmed experimentally and motivated by the on-set of additional deteriorative reactions. When due modifications were inserted in the model, its predictions performed very satisfactorily. The model has been also exercised by confirming that the adoption modified atmosphere packaging may inhibit and protect microbial growth.

Flexible design of new packaging configurations, and the verification of existing ones can be worked out by using this tool. Possible outcomes are the determination of the relationship between respiration rate and gas

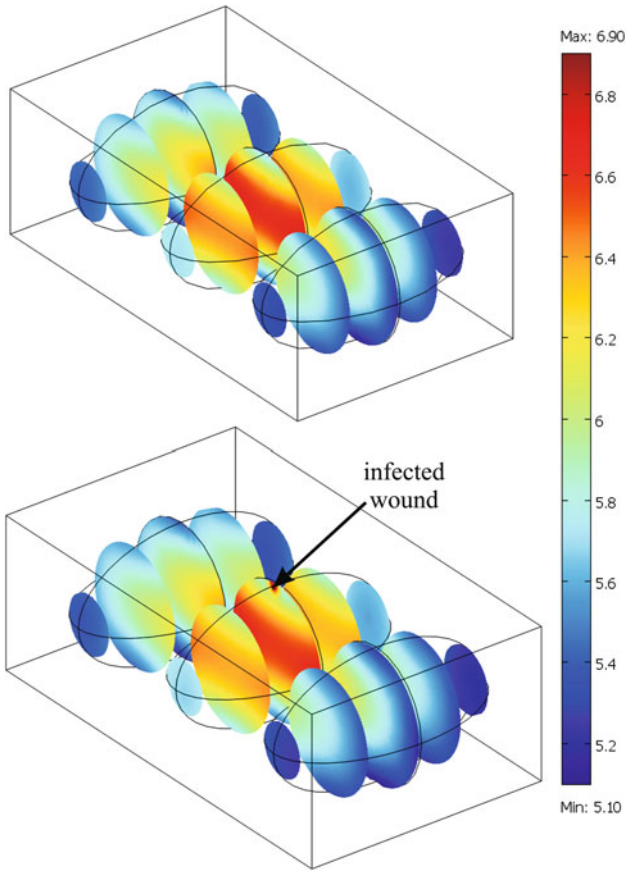

Fig. 6 *MS* CFU distributions after 13 days at $T_p = 8$ °C for pMAP, with wholesome samples (*top*) and with an infected sample (*bottom*). The modified atmosphere packaging contributes to maintain safety in the fruits

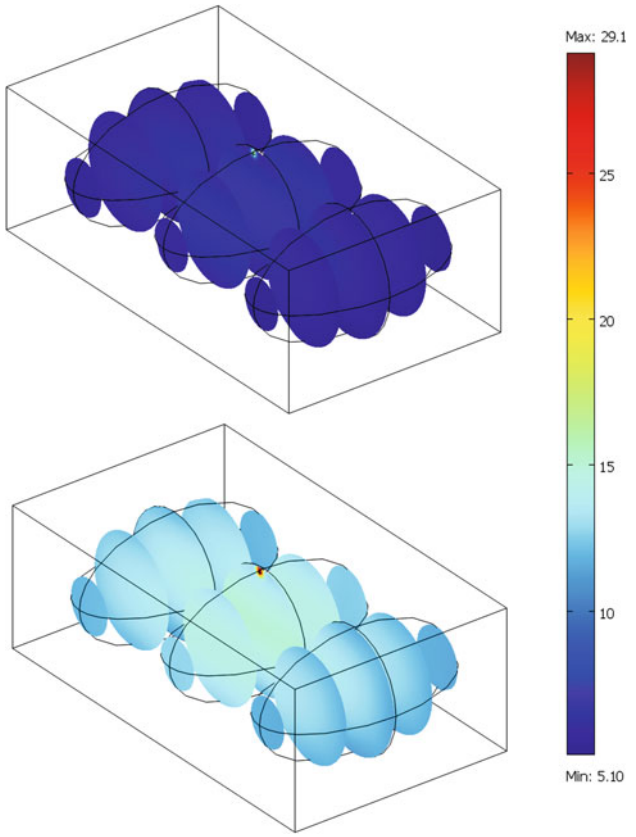

Fig. 7 *MS* CFU distributions in presence of an infected sample, after 3 (*top*) and 4 (*bottom*) days at $T_p = 8$ °C in air. The fruits stored in an open box lose rapidly their commercial value

diffusion through the film, for specific produce/material coupling, the systematic selection of the appropriate gas conditions in packaging, as well as the verification of possible microbial hazards or the design of new hurdles to microbial growth.

References

1. Bird RB, Stewart WE, Lightfoot EN (2002) Transport phenomena. Wiley, New York
2. Cefola M, Renna M, Pace B (2011) Marketability of ready-to-eat cactus pear as affected by temperature and modified atmosphere. J Food Sci Technol. doi:10.1007/s13197-011-0470-5
3. COMSOL Multiphysics user's guide, COMSOL AB (2008)
4. De Bonis MV, Ruocco G (2012) Computational transport phenomena in bioprocessing with the approach of the optimized source term in the governing equations. Heat Mass Transf. doi:10.1007/s00231-012-0992-z
5. Del Nobile MA, Baiano A, Benedetto A, Massignan L (2006) Respiration rate of minimally processed lettuce as affected by packaging. J Food Eng 74:60–69
6. Dense EJ, Van Impe JF (2001) On the need for another type of predictive model in structured foods. Int J Food Microbiol 64:247–260
7. Fonseca SC, Oliveira FAR, Brecht JK (2002) Modelling respiration rate of fresh fruits and vegetables for modified atmosphere packages: a review. J Food Eng 52:99–119
8. Jacxsens L, Devlieghere F, Devebere J (1999) Validation of a systematic approach to design equilibrium modifed atmosphere packages for fresh-cut produce. Food Sci Technol-LEB 32:425–432
9. Jacxsens L, Devlieghere F, Debevere J (2002) Predictive modelling for packaging design: equilibrium modified atmosphere packages of fresh-cut vegetables subjected to a simulated distribution chain. Int J Food Microbiol 73:331–341
10. Kader AA, Zagory D, Kerbel EL (1989) Modified atmosphere packaging of fruit and vegetables. Crit Rev Food Sci 28:1–30
11. Lammertyn J, Scheerlinck N, Jancsók P, Verlinden BE, Nicolaï BM (2003) A respiration–diffusion model for 'Conference' pears I: model development and validation. Postharverst Biol Technol 30:29–42
13. Opara LU, Zou Q (2007) Sensitivity analysis of a CFD modelling system for airflow and heat transfer of fresh food packaging: inlet air flow velocity and inside-package configurations. Int J Food Eng 3:16
13. Piergiovanni L, Limbo S (2010) Food packaging—Materiali, tecnologie e qualità degli alimenti. Springer, Milano
14. Piringer O (2011) Transport equations and their solutions. In: Piringer OG, Baner AL (eds) Plastic packaging materials for food. WILEY-VCH Verlag, Weinheim, pp 183–220

15. Saenz C (2000) Processing technologies: an alternative for cactus pear (*Opuntia* spp.) fruits and cladodes. J Arid Environ 46:209–225
16. Sandhya (2010) Modified atmosphere packaging of fresh produce: current status and future needs. Food Sci Technol-LEB 43:381–392
17. Singh RP, Heldman DR (2009) Introduction to food engineering. Academic Press, San Diego
18. Soliva-Fortuny RC, Elez-Martínez P, Martín-Belloso O (2004) Microbiological and biochemical stability of fresh-cut apples preserved by modified atmosphere packaging. Innov Food Sci Emerg 5:215–224
19. Zhang Y, Liu Q, Rempel C (2011) Mathematical modeling of modified atmosphere packaging. In: Brody AL, Zhuang H, Han JH (eds) Modified atmosphere packaging for fresh-cut fruits and vegetables. Blackwell Publishing, Oxford, pp 11–30
20. Zhuang H (2011) Introduction. In: Brody AL, Zhuang H, Han JH (eds) Modified atmosphere packaging for fresh-cut fruits and vegetables. Blackwell Publishing, Oxford, pp 3–10